

100
P-20

Overview of the NASA Dryden Flight Research Facility Aeronautical Flight Projects

Robert R. Meyer, Jr.

(NASA-TM-104254) OVERVIEW OF THE
NASA DRYDEN FLIGHT RESEARCH
FACILITY AERONAUTICAL FLIGHT
PROJECTS (NASA) 20 2

N92-31261

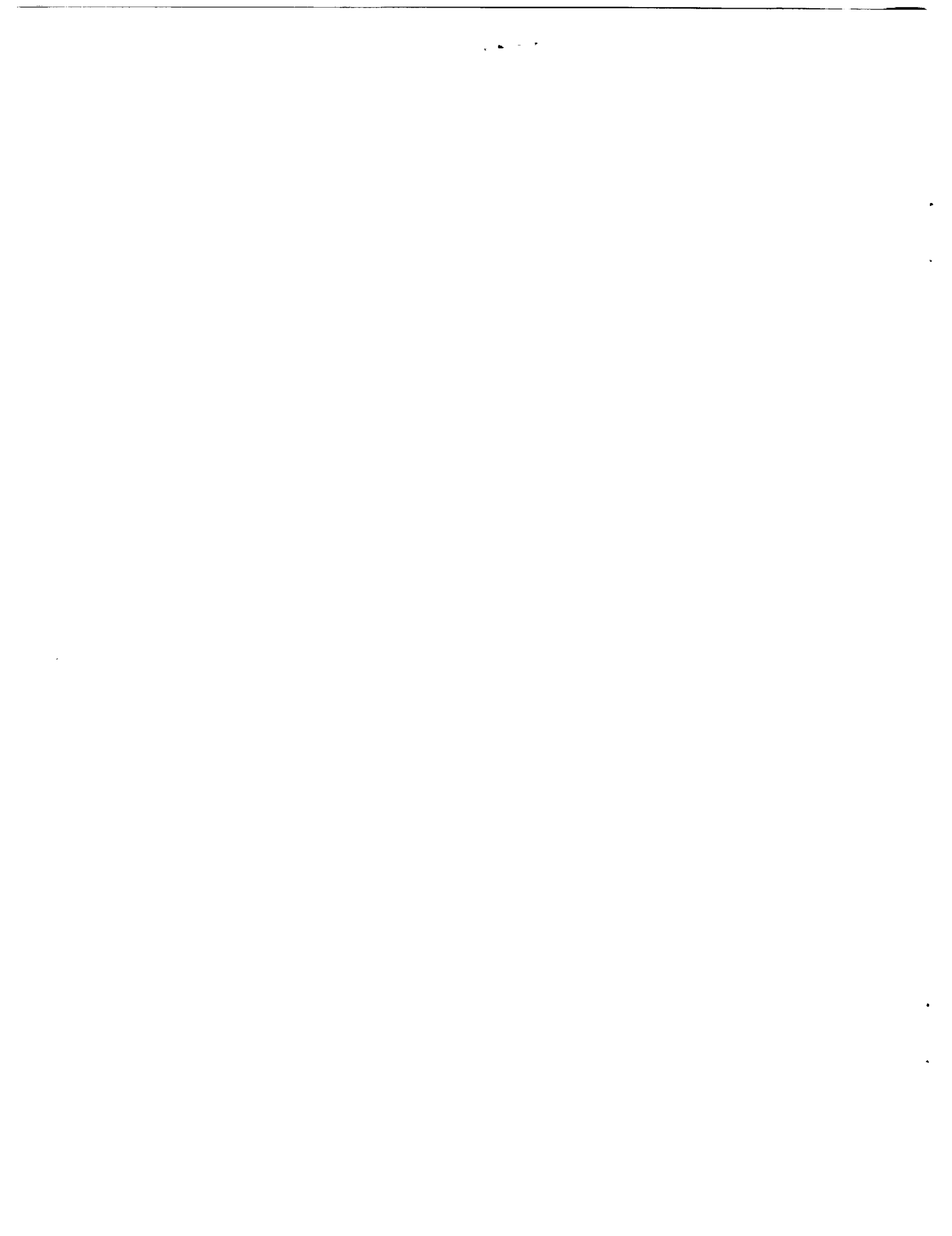
Unclas

August 1992

63/05 0115117



National Aeronautics and
Space Administration



Overview of the NASA Dryden Flight Research Facility Aeronautical Flight Projects

Robert R. Meyer, Jr.
NASA Dryden Flight Research Facility, Edwards, California

1992



National Aeronautics and
Space Administration

Dryden Flight Research Facility
Edwards, California 93523-0273

OVERVIEW OF THE NASA DRYDEN FLIGHT RESEARCH FACILITY AERONAUTICAL FLIGHT PROJECTS TESTING

Robert R. Meyer, Jr.
NASA Dryden Flight Research Facility
P.O. Box 273, D-2131
Edwards, California, USA 93523-0273

1. SUMMARY

Several principal aeronautics flight projects of the NASA Dryden Flight Research Facility are discussed. Key vehicle technology areas from a wide range of flight vehicles are highlighted. These areas include flight research data obtained for ground facility and computation correlation, applied research in areas not well suited to ground facilities (wind tunnels), and concept demonstration.

2. NOMENCLATURE

g	acceleration, 32 ft/sec ²
HARV	High Alpha Research Vehicle
Hz	frequency, cycles/sec
F.S.	fuselage station, in.
LEX	leading-edge extension
α	angle of attack, deg
β	angle of sideslip, deg
ϕ	bank angle, deg
Λ	leading-edge sweep, deg
θ	forebody cross-section angular location (0° is bottom centerline, positive is clockwise as seen from a front view, 0 to 360°), deg

3. INTRODUCTION

Flight research at the NASA Dryden Flight Research Facility is providing a surge in output for NASA's aeronautics technology program. New vehicle technologies encompassing high performance, high speed and hypersonics, and new flight-test techniques making flight research more accurate and more productive are prominent in the flight projects underway. This paper draws on recent results from several of Dryden's principal aeronautics flight projects, including the F-18 High Alpha Research Vehicle (HARV), X-29 Forward-Swept-Wing aircraft, F-15 performance seeking control (PSC), F-16XL, SR-71, and the Pegasus[®] add-on research experiments, all in productive flight phases either currently or in the recent past.

Technical highlights from these flight projects are cited to illustrate explorative flight research for aeronautical technologies dependent on flight. These technologies include extreme envelope aerodynamics and maneuvering, integrated propulsion-airframe controls, and exploration of local flow aerodynamics and aerothermal effects in the hypersonics regime.

Whereas these flight programs illustrate aeronautical technology areas, the test techniques and measurement technologies are important outputs of flight research that allow more precise measurements and improved efficiency or productivity in flight test. Thus, examples of improved tools and techniques will be described as they are used on the various flight projects.

4. F-18 HIGH ALPHA RESEARCH VEHICLE

The F-18 HARV is the flight research vehicle for NASA's High Angle of Attack Technology Program (HATP) [1]. The F-18 HARV flight research program has been divided into three phases, as shown in figure 1. Phase 1 of the flight research program was oriented toward fluid mechanics, flight mechanics, and airdata associated with high-angle-of-attack flight. Phase 2 is underway and includes the incorporation of thrust vectoring vanes in the exhaust of each engine, as well as another flight-control computer to house custom control laws. This computer commands thrust vectoring vanes and conventional aerodynamic controls to enable controlled flight at high angles of attack. Phase 3 will conduct research in high-angle-of-attack control by manipulation of the forebody vortices.

4.1. Phase 1 Aerodynamic Results

The previously obtained Phase 1 high-angle-of-attack aerodynamic results investigated forebody and leading-edge extension (LEX) aerodynamics (including on- and off-surface flow visualization), airdata

[®]Pegasus is a registered trademark of Orbital Sciences Corp., Fairfax, Virginia.

measurement techniques, wing surface flow visualization, and vertical tail buffet, as shown in figure 2. A primary task was to correlate flight flow visualization results with water tunnel, wind tunnel, and computational results. An example of on-surface (tufts) and off-surface flow visualization using a smoke system [2] is shown in figure 3. The figure shows smoke emitted from ports at the side of the forebody and LEX simultaneously. The smoke illuminates the forebody and LEX vortices. These vortices have a significant effect on the high-angle-of-attack flight characteristics of the aircraft, and a major effort of the program has been to model these vortices, using computational methods [3]. Another flow visualization technique uses an emitted dye technique and is shown in figure 4. This technique highlights on-surface streamlines and can be used to identify fluid mechanic characteristics such as separation and attachment lines. This technique has been extremely useful for computational code correlation and interpretation of pressure data.

Figure 5 shows the diagnostics available from the on-surface emitted dye technique [4]. Shown in the figure is a side view of the surface streamlines at an angle of attack of 47° . Visible in the view at a theta of approximately 240° is a puddling of the emitted fluid, indicating a laminar-to-turbulent flow separation bubble. This indication is supported by close examination of the flow or streamlines downstream of roughness from screwheads (noted in figure), where the local flow has tripped to a turbulent condition and the puddling, or laminar separation is not evident downstream of the screwheads. This unexpected laminar separation bubble establishes the presence of laminar flow on the forebody.

The discovery of laminar flow on the forebody at high-angle-of-attack flight conditions was contrary to previous understanding. In fact, computational models were assuming turbulent flow on the forebody. Wind-tunnel testers attributed differences in flight and wind-tunnel forebody results to the presence of laminar flow in the wind tunnel and its absence during flight.

Figure 6 presents an example of the type of correlation made from the off-surface flow visualization flight results from reference 5. The figure shows the LEX vortex burst location as non-dimensional fuselage length, plotted against angle of attack for flight and water-tunnel experiments. Photo insets show the flight LEX vortex burst for two angles of attack. The

water tunnel and flight burst location results agree very closely, an unexpected result.

Another interesting correlation is shown in figure 7, where flow visualization results are correlated with vertical tail buffet data [1]. The figure presents normalized vertical tail accelerations plotted against angle of attack. Two structural modes are shown in the figure, one at the vertical tail first bending frequency of 15 Hz and another at the vertical tail second bending frequency of 44 Hz. The 15-Hz mode shows the most vertical tail acceleration and reaches a maximum at an angle of attack of approximately 30° . Photo insets show the visualization of the LEX vortex, which is believed to be the primary source of the unsteady flow impinging on the vertical tail. It is interesting to note the position of the vortex burst point for the two photos. The photo representing $\alpha = 20^\circ$ shows vortex burst slightly forward of the vertical tail, while the photo for $\alpha = 30^\circ$ (maximum acceleration) shows vortex burst a significant distance forward of the vertical tail. One explanation for the forward burst location imparting more acceleration or buffet to the vertical tail is related to the diameter of the burst vortex relative to the vertical tail span. At $\alpha = 30^\circ$ the burst vortex diameter is approximately equal to the vertical tail span, and excites the first bending mode at 15 Hz. At $\alpha = 20^\circ$, the burst vortex core is a small percentage of the span, thus affecting a smaller portion of the vertical tail and exciting the higher frequency second bending mode at 44 Hz.

4.2. Phase 2 Thrust Vectoring and Flight Control Research

The F-18 HARV recently completed the envelope expansion of the pitch and yaw thrust vectoring system. The standard F404 external nozzles were removed to incorporate three airframe-mounted turning vanes per engine. These turning vanes deflect the exhaust path, thereby providing reaction forces and moments [6]. Although this system is not optimized for weight or aerodynamic drag, it does provide an economical and effective research capability, allowing controlled flight to higher angles of attack than possible with the standard controls.

This capability provides stabilized flight for characterization of the forebody vortical flows and on-surface pressures distribution for direct comparison with ground-based prediction methods. Figure 8 presents a comparison of the stabilized flight envelope with and without thrust vectoring. Without thrust vectoring, the F-18 HARV is capable of stable flight to

slightly more than 30° -angle of attack, where moderate wing rock is encountered. The small region near 50° -angle of attack on the figure indicates an area where the wing rock diminishes in magnitude and the aircraft is minimally stable. With thrust vectoring, the aircraft has demonstrated stable flight through $\alpha = 70^\circ$.

The thrust vectoring capability also allows more controlled flight at high angles of attack, where primary interest lies in the improved handling qualities and extreme envelope dynamic maneuvers. An example of stabilized flight with thrust vectoring is shown in figure 9 [6] for time histories of bank angle, angle of sideslip, and roll and yaw rate in the wing rock region near 40° -angle of attack. Figure 9(a) presents data without thrust vectoring and shows typical F-18 wing rock in this region. Figure 9(b) shows the same maneuver at the same flight conditions with thrust vectoring and that the wing rock is almost eliminated.

5. X-29 FORWARD-SWEPT WING

The X-29 Forward-Swept-Wing aircraft (fig. 10) sponsored by the Defense Advanced Research Projects Agency (DARPA), the Air Force, and NASA has completed the low-speed high-angle-of-attack envelope expansion and military utility portion of the flight program (Phase 1) [7]. High-angle-of-attack aero characterization studies were conducted to study forebody contributions to overall vehicle aerodynamics, wing canard interaction, and forebody vortex interaction with the vertical tail. Flow visualization and pressure techniques similar to those on the F-18 HARV were used to investigate the forebody aerodynamics and flow interactions between the canard and wing. Here, the forebody vortex (not the LEX) burst location relative to the vertical tail is of particular interest because it can lead to tail buffet problems.

Figure 11 (from ref. 8) summarizes the general high-angle-of-attack flight characteristics of the X-29A. The most notable characteristic of the aircraft is excellent pitch control, particularly positive nose-down authority, even up to the maximum angle of attack obtained of 66° . Light buffet began at $\alpha = 13^\circ$, increased in magnitude to moderate buffet by $\alpha = 20^\circ$, and continued up to the maximum angle of attack obtained of 66° . Another feature of the X-29A was its excellent roll control and coordination, which was up to almost 40° -angle of attack. A distractor in the roll axis was a random wing drop near 20° -angle of attack and mild wing rock above 40° -angle of attack. In the yaw axis, no flying quality anomalies occurred below

40° -angle of attack, although the vertical tail encountered buffet near 30° -angle of attack. Unlike the F-18, which attributed vertical tail buffet to the LEX vortex, the X-29 vertical tail buffet problems were attributed to the forebody vortex. Above 40° -angle of attack, the X-29 encountered a nose-right yawing moment asymmetry, which changed to a nose-left asymmetry by 50° -angle of attack. Both asymmetries were marginally controllable with extreme pilot compensation. The cause for these asymmetries is discussed in the following.

Figure 12 correlates three measurements obtained from zero sideslip maneuvers. The first source was the overall aircraft zero sideslip yawing moment from flight data (solid line, ref. 7). The second source was the zero sideslip nominal angle of the forebody vortex pair (referenced to the vertical) obtained from a vertical tail camera during forebody smoke tests (triangle symbols, ref. 9). The nominal angle of the forebody vortex is referenced to the right ordinate. The third source was resulting moments obtained by integrating the four rings of forebody pressure orifice data (circular symbols, ref. 10) at zero sideslip. The aircraft data (solid line) show a nose-right moment at about 45° -angle of attack, followed by a nose-left moment by 50° -angle of attack, as previously discussed. The forebody vortex nominal angle (θ_v) using the scale on the right side of the plot shows the same trends as the aircraft data. The vortex angle data indicate that the yawing moment asymmetry is related to the forebody vortex. However, the moment obtained from the integrated pressures (triangle symbols) does not indicate the nose-right moment near 45° -angle of attack, but does indicate the nose-left moment by 50° -angle of attack. The pressure data show that the yawing moment is not a result of the forces acting on the forebody itself, although the asymmetry in the vortex flow originates on the forebody as shown from the vortex angle data (θ_v). In summary, the aircraft and forebody vortex position (smoke) data show the same trends, while the integrated forebody pressures do not indicate the initial nose-right yaw moment at 45° .

The data in figure 13 show one possible explanation for this anomaly. Figure 13 presents forebody section integrated pressure yawing moment data for a forward section (solid line) and the most aft section (dashed line) as shown in the inset. The forward section data (solid line) follow the same trend as the overall forebody integration discussed in the previous figure. However, the most aft section indicates a mild trend toward a nose-right moment at about 45° -angle

of attack and less tendency for a nose-left moment above 50°- angle of attack. Extrapolating this data aft on the aircraft fuselage would indicate that the nose-right moment at about 45°-angle of attack is the probable result of forces and moments from the cockpit, canopy, or area farther aft for which pressure data were not obtained. Recalling that the forebody vortex angle from the smoke visualization tracked the nose-right and nose-left asymmetry but the integrated forebody pressures did not, the data from figure 13 indicate that the nose-left asymmetry is the indirect result of the forebody vortex asymmetry interacting downstream of the forebody on the canopy-cockpit area.

6. F-15 PERFORMANCE SEEKING CONTROLS

Integrated propulsion-airframe control technology is the principal focus of the F-15 PSC program. Digital algorithms to estimate specific engine characteristics, including effects of engine wear and day-of-flight environmental conditions, allow onboard optimization of engine-airframe performance [11]. The program has been divided into two phases: subsonic testing, which was started in 1990 and finished in 1991 and supersonic testing, which started early in 1992 and is expected to continue through 1993. The aircraft has been modified to incorporate an additional digital computer to execute the PSC control laws.

Figure 14 contains subsonic flight results [11] that show performance differentials between the PSC system engaged and disengaged for three different modes of operation. There are two constant thrust modes; one that minimizes temperature and a second that minimizes fuel consumption. There is also a maximum thrust mode. In the maximum thrust mode, the system increased thrust by a maximum of 12 percent, while in the minimum temperature mode, turbine inlet temperature was decreased by a maximum of 100 °F. In the minimum fuel mode, specific fuel consumption was decreased by a maximum of 1.7 percent. While this flight research activity was conducted on a fighter-type aircraft (F-15), this research activity is considered dual role, in that the results are applicable to high-performance military and civil transport applications.

7. SR-71 TESTBED

The SR-71 is one of two high-speed testbed aircraft at Dryden, the other being the F-16XL. With its large Mach number envelope and large size, the SR-71

provides unique opportunities for conducting research in support of the nation's high-speed transport and hypersonic research programs. One such experiment planned for 1993 and 1994 is in support of the National AeroSpace Plane (NASP) hypersonic vehicle [12]. Figure 15 is an artist's conception of a scale portion of the NASP nozzle cowl design mounted on top of the SR-71A. The test concept involves base drag reduction of the blunt aft vehicle geometries of airbreathing hypersonic vehicles at transonic speeds using external burning. Hydrogen fuel for the external burning tests will be contained in the chine region of the aircraft. Testing will be conducted between Mach numbers of .8 to 2.5. The planned tests will obtain valuable data on fuel ignitors, flame holders, scale effects, and operational considerations using hydrogen as a fuel. These data are expected to influence the design of the full-scale system.

Figure 16 indicates some advantages of flight testing this concept. The graph shows the operating envelope for the SR-71A testbed in terms of altitude and Mach number. The shaded area represents the nominal aircraft envelope and the cross-hatched area represents plans to extend the current SR-71 aircraft envelope. In addition, the operating envelope includes the proposed wind-tunnel test points (solid symbols) and the expected minimum static pressure limit of 2 lb/in² for external burning stable combustion.

The advantages of flight test include a large test envelope, potential for large test articles, and a more realistic test environment. The test envelope covers a larger range of Mach numbers than can be obtained in a single wind tunnel. For these tests, data probably will not be obtained for Mach numbers much greater than 2.5, because at about Mach 2.5 the aircraft altitude will exceed the minimum pressure of 2 lb/in² for stable external burning combustion.

Although the aircraft could support larger test articles, the current test fixture is the same size and shape as the proposed wind-tunnel model, since there are no wind-tunnel wall interference concerns associated with the aircraft. The aircraft tests also allow for a more realistic test environment (including transient conditions) which might involve transitions across the 2 lb/in² stable combustion limit or Mach sweeps rather than selected discrete test Mach numbers. Other realistic test conditions include the effects of freestream atmospheric turbulence (which cannot be simulated in the wind tunnel) and a capability to vary flow angle, which is not planned in wind-tunnel tests.

8. F-16XL TESTBED

The F-16 XL is an F-16 aircraft which was modified by the addition of a cranked arrow wing, as shown in the planform photo of figure 17. Only two of the aircraft were built and NASA is using them both for supersonic flight research. A major research goal with the aircraft is to attain significant amounts of laminar flow on highly swept planforms typical of supersonic aircraft. Laminar flow studies are usually not well suited for wind tunnels because of wind-tunnel freestream disturbances (noise), scale effects, and model size limitations. The total laminar flow research program extends through the late 1990's and involves testing a series of larger chord laminar flow test sections, or gloves, installed on the wing of the F-16XL.

The first laminar flow glove section flight tested [13] is shown installed on the left wing (fig. 17). The active portion of the test section is the midspan dark area extending aft from the leading edge. It is surrounded by a passive glove fairing (shown in white), which smoothly fairings the test section with the remainder of the wing. To attain laminar flow on the highly swept leading edges typical of supersonic aircraft, active boundary-layer control using suction is usually required. The skin of the test section is a porous, perforated titanium skin, which allows the boundary layer to be removed, or sucked off, as necessary. The suction system hardware is contained in a fuselage compartment, identified in figure 17. Plumbing lines between the suction system and the test section are contained beneath the passive glove.

Results from the first laminar flow glove, flight tested in 1991 and 1992, are shown in figure 18. The outlines represent the perforated titanium test section, with the shaded areas showing laminar flow attained. The test section outline on the left side of the figure shows results with suction and the right test section outline represents results without suction. The symbols on the test section represent the locations of hot films used to determine the state of the boundary layer (laminar or turbulent).

The figure shows a significant difference in laminar flow attained with and without suction. With suction, most of the test section boundary layer was maintained in a laminar state, while without suction only a small part on the leading edge was laminar. These data represent the most known laminar flow obtained in-flight at supersonic speeds for a leading-edge sweep of 70° .

9. PEGASUS ADD-ON HYPERSONIC RESEARCH

The Pegasus air-launched orbital insertion system provides opportunities to conduct hypersonic fluid and flight mechanics research in an add-on or piggyback fashion during normal orbital insertion missions [14]. The Pegasus is a three-stage-to-orbit launch system, not including the NASA Dryden B-52 launch carrier vehicle, as shown in figure 19. The first stage of the launch system is a winged, aircraft-like vehicle which separates from the remainder of the vehicle at approximately Mach 8 and 200,000-ft (61 km) altitude. The first stage, with its wings and aero surfaces for stability and control, provides interesting opportunities for add-on hypersonic investigations. Another feature is that the weight added to the first stage for instrumentation has a small impact on the final payload weight allowed.

To date, data have been obtained on two launches of the vehicle. Investigations have included temperature, heat flux, and pressure measurements, as well as trajectory reconstruction for performance evaluation. Figure 20 shows representative time histories of temperature measurements from the fillet at the wing fuselage juncture, as depicted in the inset. By comparing the two graphs, a significant temperature difference between the two sensors is shown. This difference demonstrates the problem associated with making measurements on an as-built flight vehicle. The top graph presents results from various depths of the as-built Pegasus structure, which consisted of an ablative, insulator, and graphite epoxy structure. These temperatures are expected to be lower because of the presence of the ablator, from which heat flux values are difficult to extract. The lower graph shows results from a thermocouple mounted atop a specially installed plug of space shuttle thermal protection system tile. The tile material is a well-documented insulator and provides an excellent measurement system for extracting heat flux values. The shuttle tile plugs provide a highly responsive measurement of changes in local heat flux, but the absolute value of the measurement does not represent the as-built structure. The study just described provided insight for temperature and heat flux measurement methods on as-built hypersonic vehicles and will be used on subsequent hypersonic flight programs.

10. CONCLUDING REMARKS

Flight research encompassing a wide range of flight vehicles is summarized, with principal results in

key vehicle technology areas identified. These areas included flight programs that spanned the speed range from low-speed, high-angle-of-attack programs focused on maneuverability, to hypersonic speeds. Flight research data were obtained to compare and validate computational and ground facilities, to conduct applied research in areas not well suited to ground facilities, and for concept demonstration. Several examples are discussed where detailed fluid mechanic flight measurements have increased the understanding of aircraft component contributions to the overall aircraft flight dynamics. In addition, examples of improved tools and techniques (such as the smoke flow visualization) were described.

11. REFERENCES

- ¹Schneider, Edward T. and Robert R. Meyer, Jr., "F-18 High Alpha Research Vehicle: Description, Results, and Plans," Society of Experimental Test Pilots (SETP) 33rd Symposium Proceedings, Sept. 1989.
- ²Fisher, David F., John H. Del Frate, and Fanny A. Zuniga, Summary of In-Flight Flow Visualization Obtained from the NASA High Alpha Research Vehicle, NASA TM-101734, 1991.
- ³Rizk, Yehia M. and Ken Gee, "Numerical Prediction of the Unsteady Flowfield Around the F-18 Aircraft at Large Incidence," AIAA 92-0020, 29th Aerospace Sciences Meeting, Reno, NV, Jan. 1991.
- ⁴Fisher, David F., David M. Richwine, and Daniel W. Banks, Surface Flow Visualization of Separated Flows on the Forebody of an F-18 Aircraft and Wind-Tunnel Model, NASA TM-100436, 1988.
- ⁵Del Frate, John H. and Fanny A. Zuniga, "In-Flight Flow Field Analysis on the NASA F-18 High Alpha Research Vehicle with Comparisons to Ground Facility Data," AIAA-90-0231, Jan. 1990.
- ⁶Regenic, Victoria, Donald Gatlin, Robert Kempel, and Neil Matheny, "The F-18 HARV - A High Angle-of-Attack Testbed Aircraft," AIAA-92-4120, Aug. 1992.
- ⁷Pellicano, Paul, Joseph Krumenacker, and David Vanhoy, "X-29 High Angle-of-Attack Flight Test Procedures, Results, and Lessons Learned," Society of Flight Test Engineers (SFTE) 21st Symposium Proceedings, Garden Grove, CA, Aug. 1990.
- ⁸Ishmael, Stephen D., Dana Purifoy, Rogers E. Smith, and Rod Womer, "X-29 High Angle of Attack," Society of Experimental Test Pilots (SETP) 34th Symposium Proceedings, Beverly Hills, CA, Sept. 1990.
- ⁹Del Frate, John H. and John Saltzman, "In-Flight Flow Visualization Results from the X-29A Aircraft at High Angles of Attack," AIAA-92-4102, Sept. 1992.
- ¹⁰Fisher, David F., David M. Richwine, and Stephen Landers, "Correlation of Forebody Pressures and Aircraft Yawing Moments on the X-29A Aircraft at High Angles of Attack," AIAA-92-4105, Aug. 1992.
- ¹¹Gilyard, Glenn B. and Orme, John S., "Subsonic Flight Test Evaluation of a Performance Seeking Control Algorithm on an F-15 Airplane," AIAA-92-3743, July 1992.
- ¹²Hicks, John W., "Development of a Hydrogen External Burning Flight Test Experiment on the NASA Dryden SR-71A Aircraft," SAE-920997, Apr. 1992.
- ¹³Anderson, Bianca T. and Marta Bohn-Meyer, "F-16XL Supersonic Laminar Flow Research," SAE-921994, Oct. 1992.
- ¹⁴Meyer, Robert R., Jr., Robert E. Curry, and Gerald Budd, "Aerodynamic Flight Research Using the Pegasus Air-Launched Space Booster," AIAA-92-3990, July 1992.

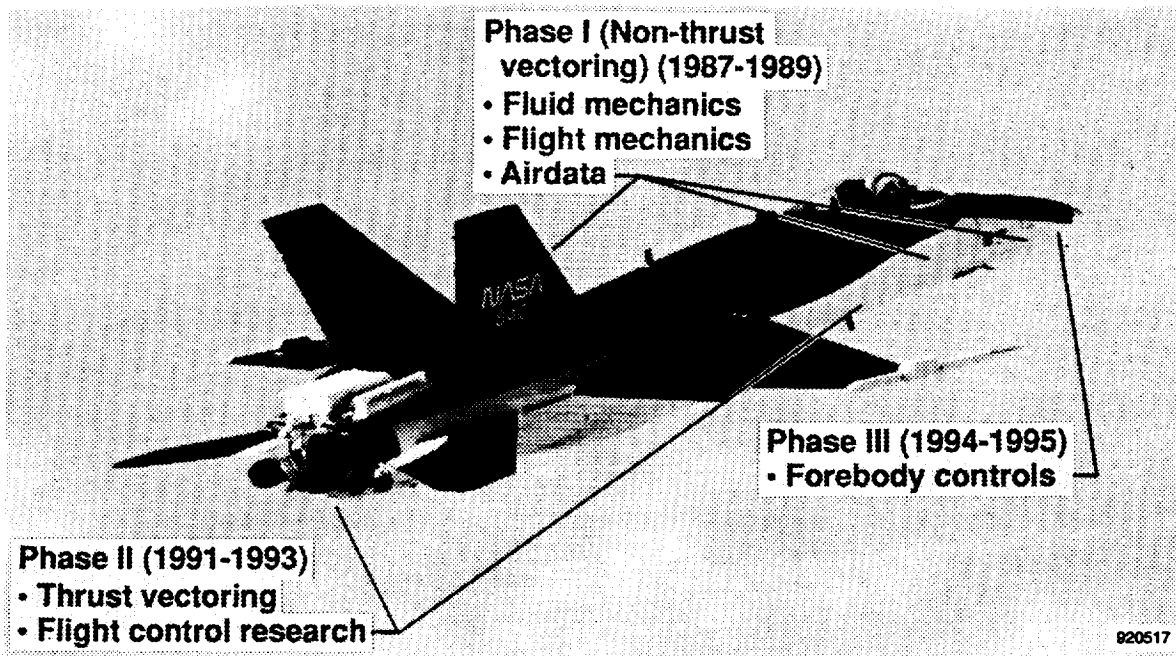


Fig. 1 F-18 High Alpha Research Vehicle program description.

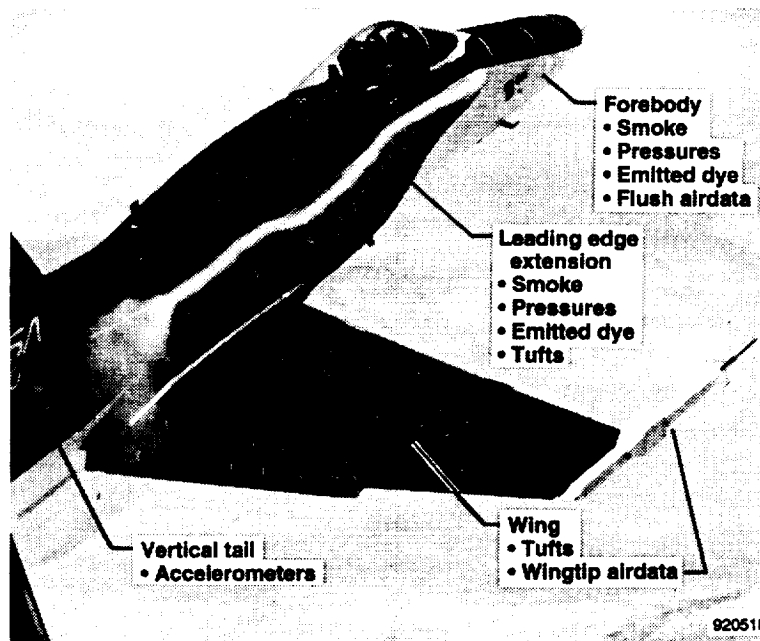


Fig. 2 Fluid mechanic experiment methods of phase 1, using the F-18 HARV.

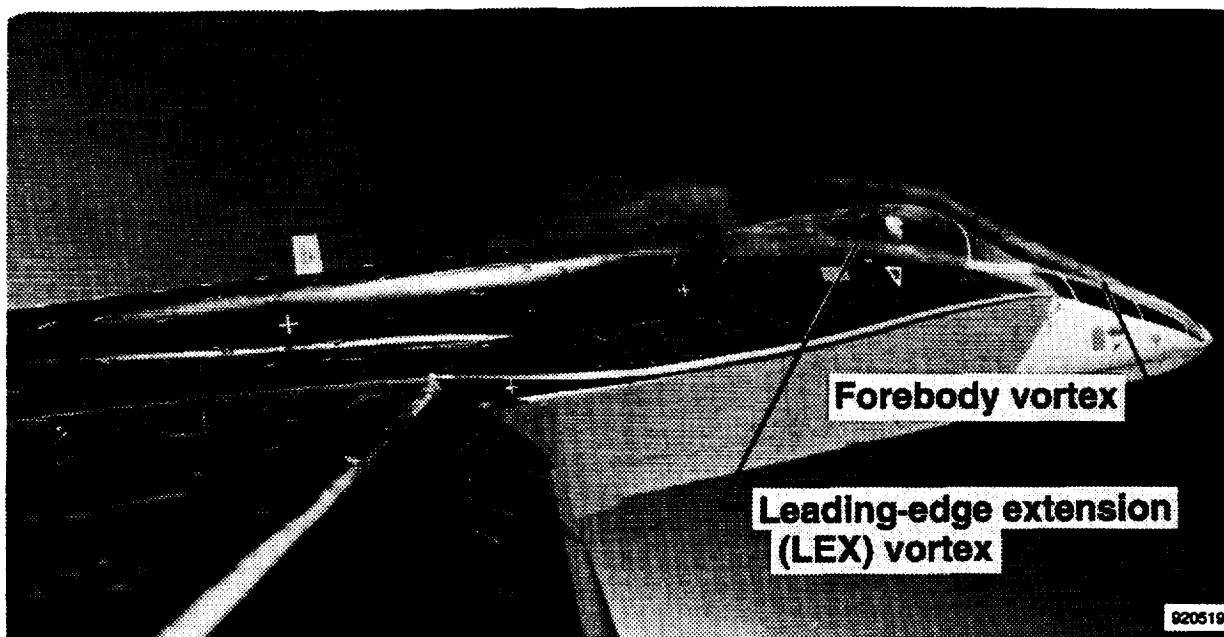


Fig. 3 Flow visualization technique, $\alpha = 32^\circ$ (F-18 HARV).

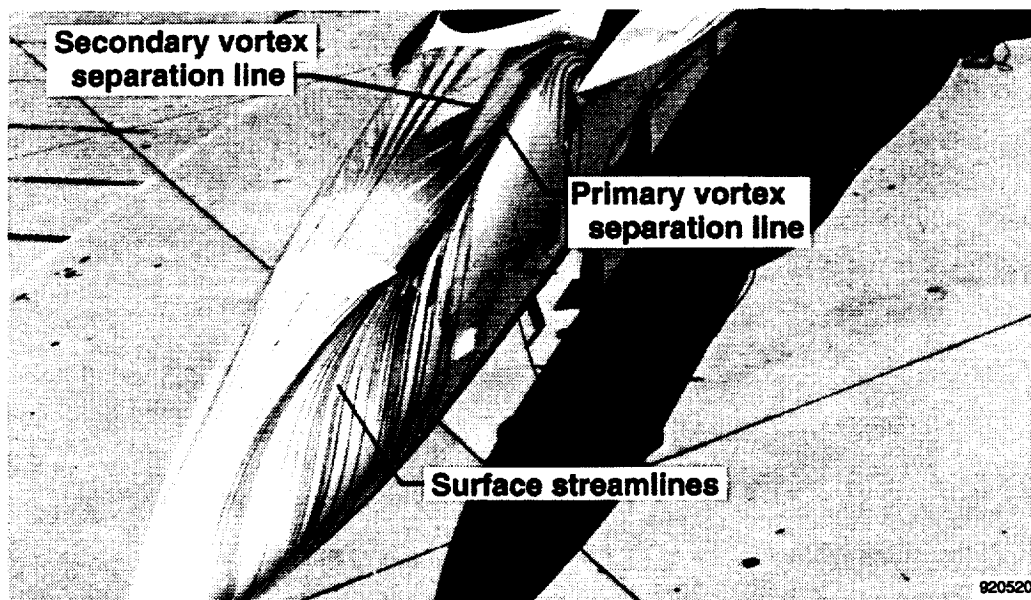


Fig. 4 Forebody on-surface flow visualization technique on F-18 HARV. (emitted dye pattern shown obtained at $\alpha = 30^\circ$).

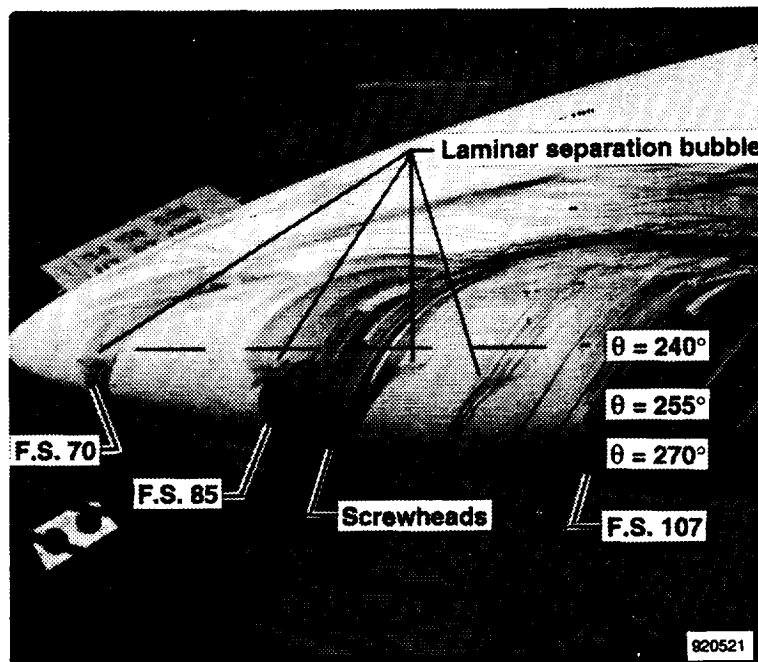


Fig. 5 Forebody surface flow at $\alpha = 47^\circ$, obtained on F-18 HARV.

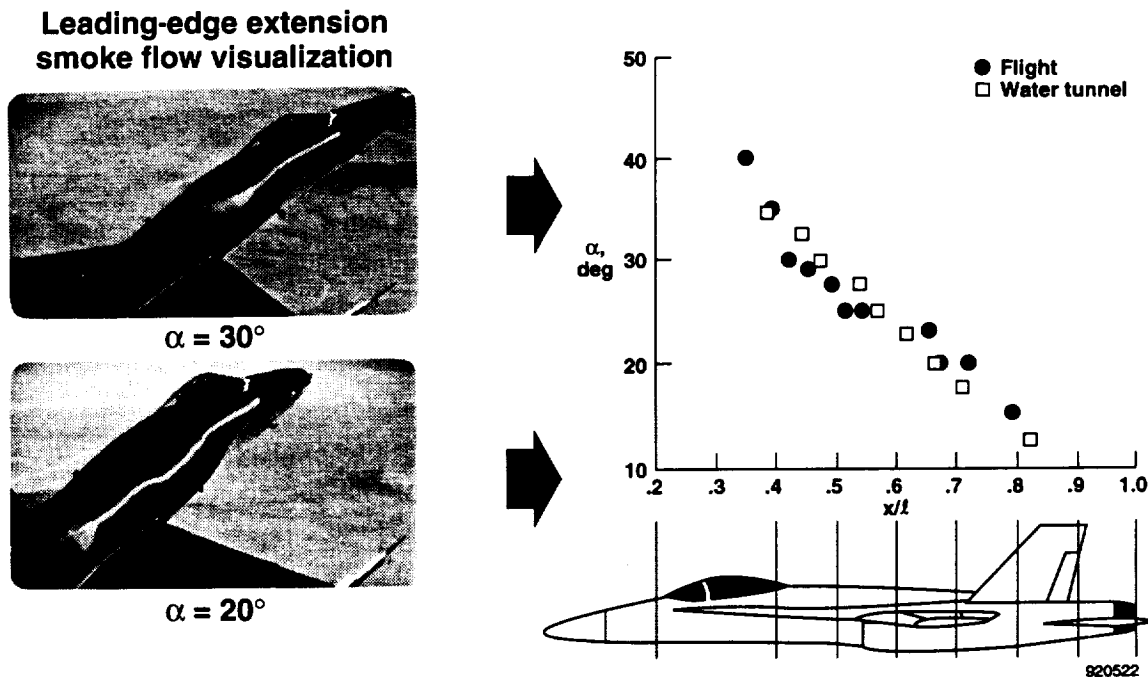


Fig. 6 Location of F-18 leading-edge extension vortex burst as a function of angle of attack from flight and water tunnel.

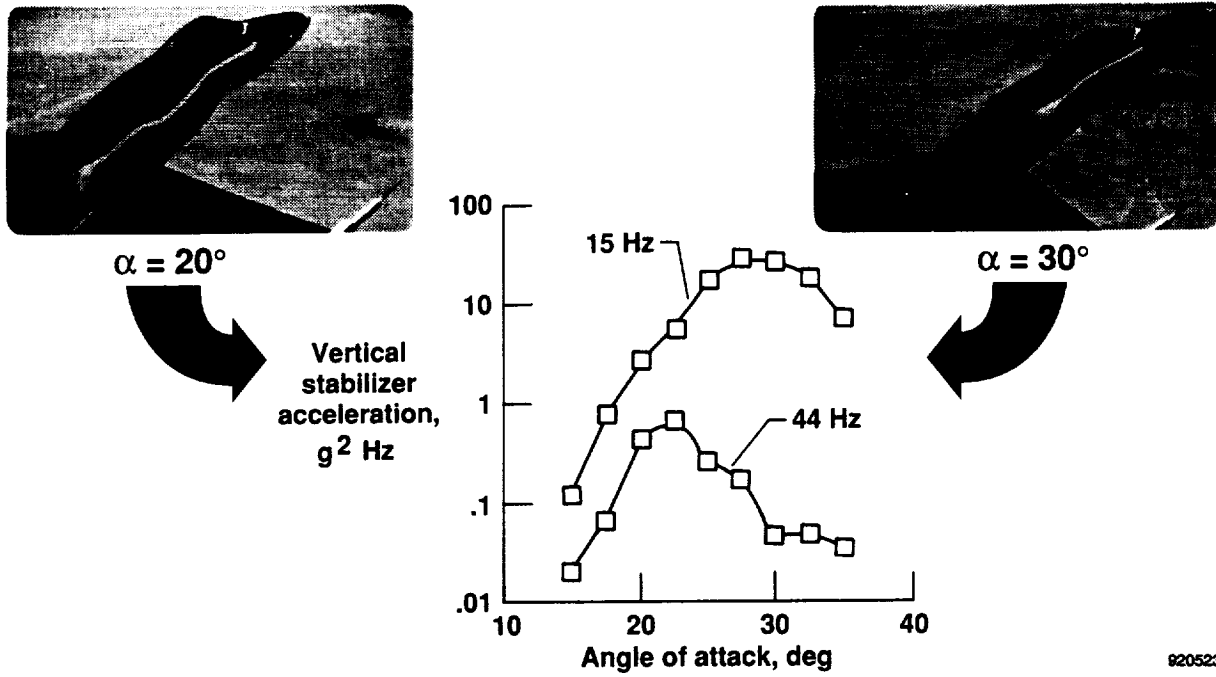


Fig. 7 Correlation of vortex burst location and vertical tail buffet for the F-18 aircraft.

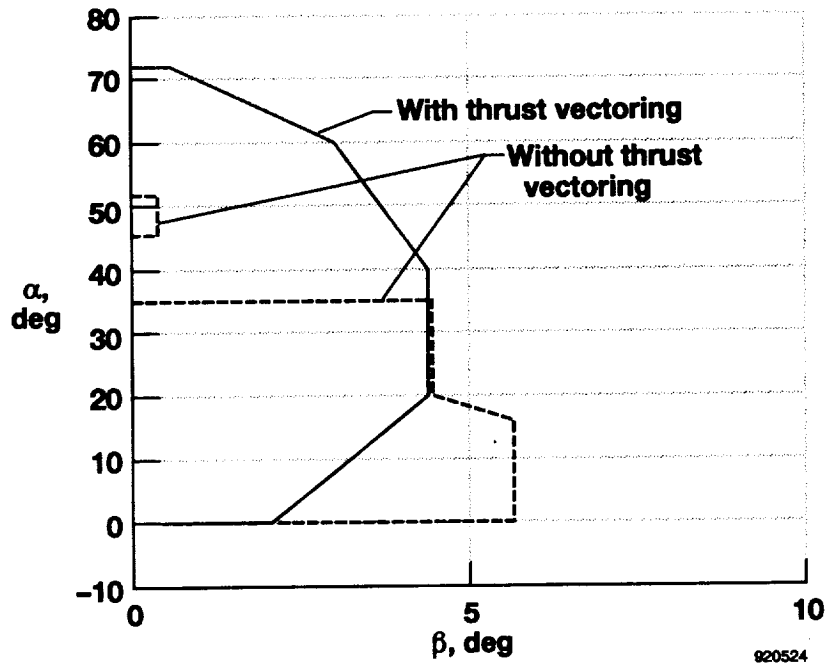
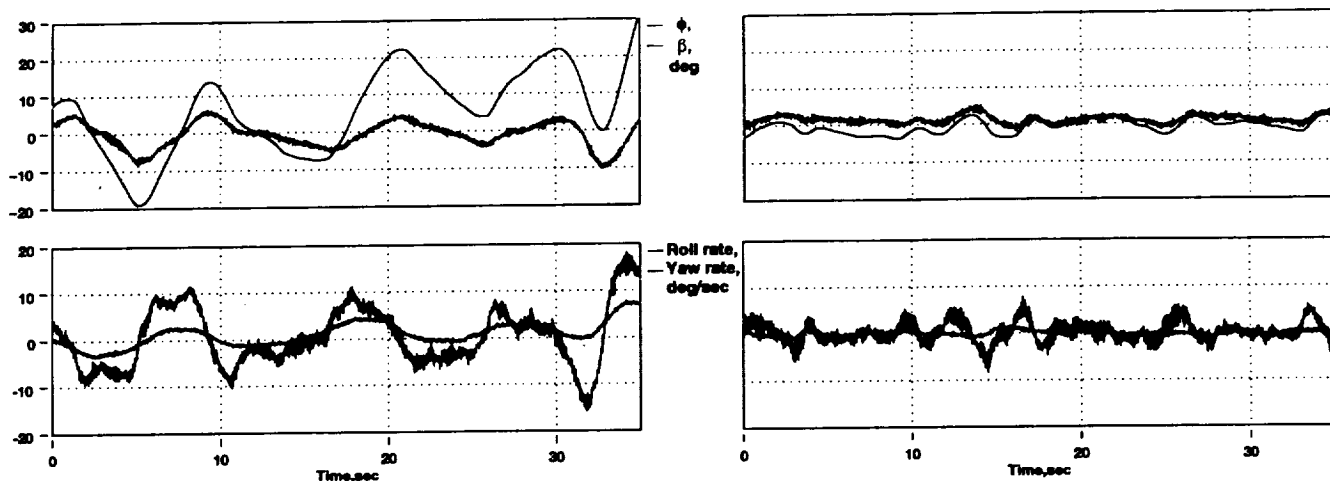
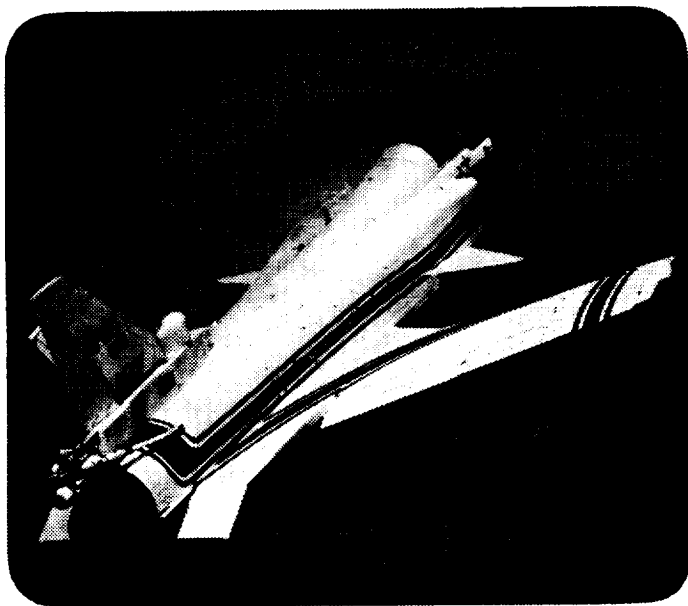


Fig. 8 Angle of attack - angle of sideslip envelope for the F-18 HARV at low speeds.



(a) Thrust vectoring off.

(b) Thrust vectoring on.

Fig. 9 The effect of thrust vectoring on the wing rock characteristics of the F-18 HARV, $\alpha = 40^\circ$.**Phase I (1989-1991)**

- Envelope expansion
- Vehicle characterization
 - Maneuverability
 - Aero derivative extraction
- Local aero characterization
 - Forebody pressures
 - Forebody smoke
 - Wing and vertical tail tufts

Phase II (1992)

- Forebody pneumatic controls

920527

Fig. 10 X-29 high-angle-of-attack program description showing forebody vortex smoke visualization.

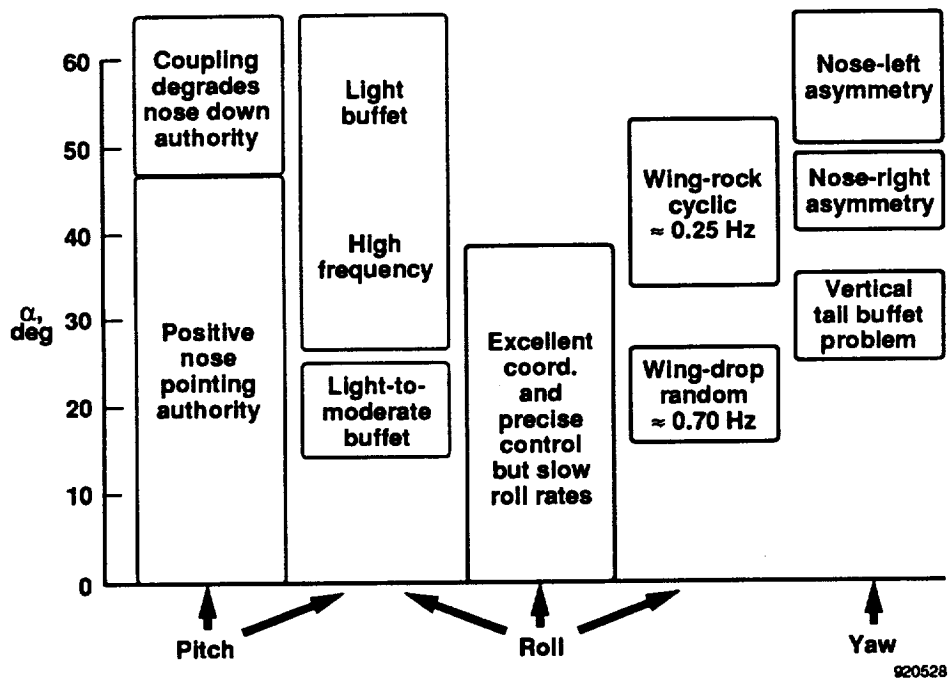


Fig. 11 High-angle-of-attack flight characteristics at low speed for the X-29 Forward-Swept-Wing aircraft.

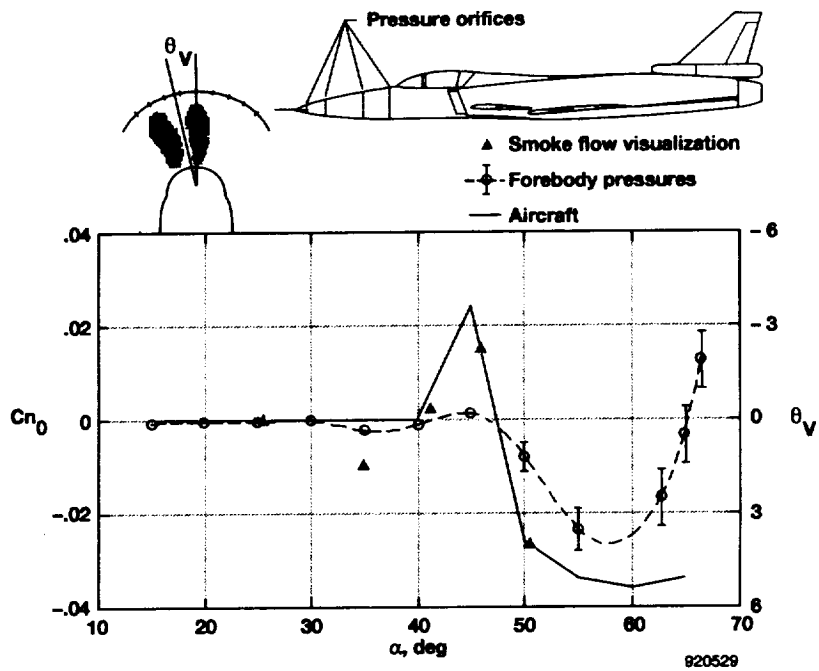


Fig. 12 High angle of attack, correlation of yawing at $\beta = 0$, low speed, for X-29A

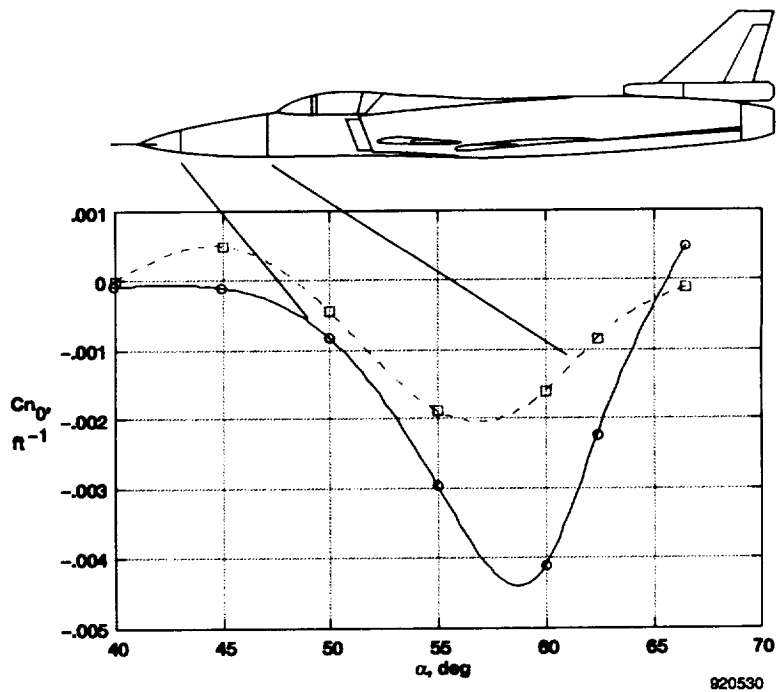
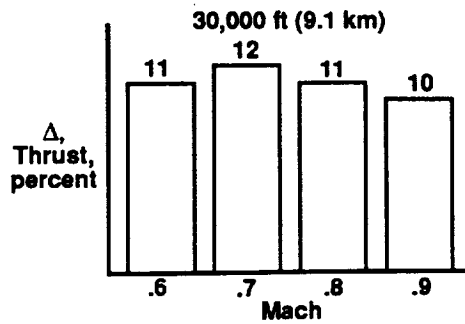
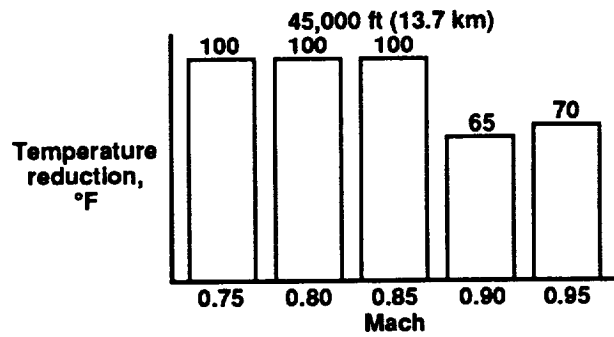


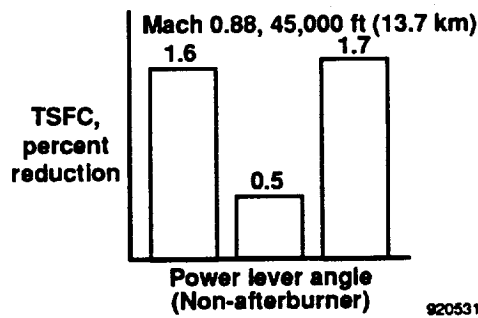
Fig. 13 High angle of attack, forebody section yawing moment, at low speed for the X-29A.



(a) Maximum thrust mode.

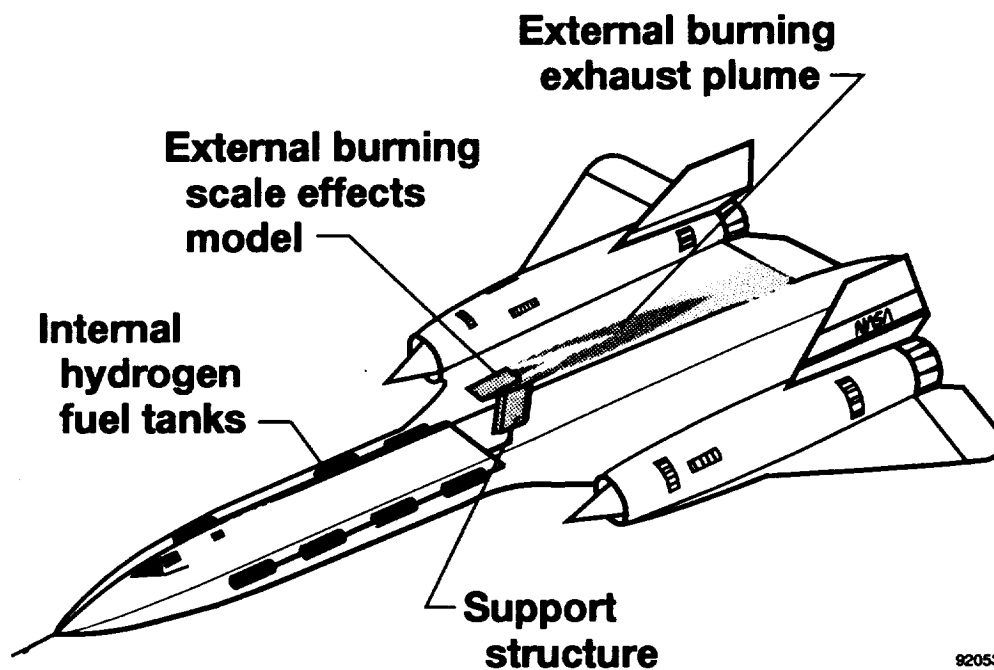


(b) Constant thrust, minimum temperature mode.



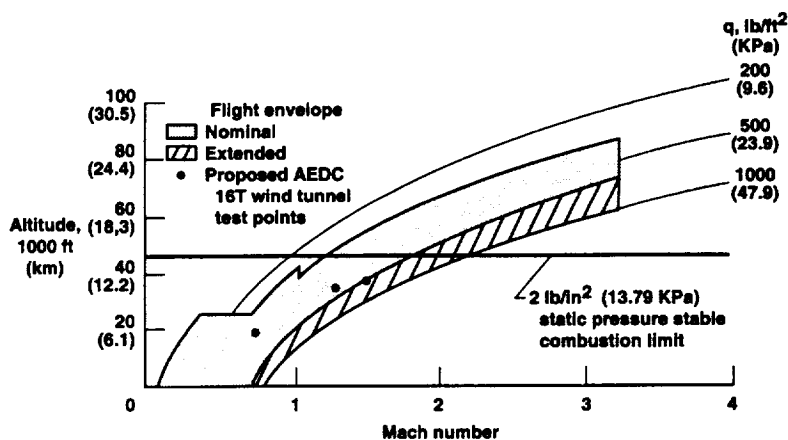
(c) Constant thrust, minimum fuel mode.

Fig. 14 Representative subsonic performance realized using performance seeking controls on the F-15.



920532

Fig. 15 High-speed external burning experiment configuration on SR-71 carrier aircraft.



- Large test envelope
- Large test article
- More realistic environment
 - Transient conditions (M,Rn)
 - Atmospheric turbulence
 - Vary flow angle

920533

Fig. 16 Flight and wind-tunnel test envelopes for the external burning experiment.

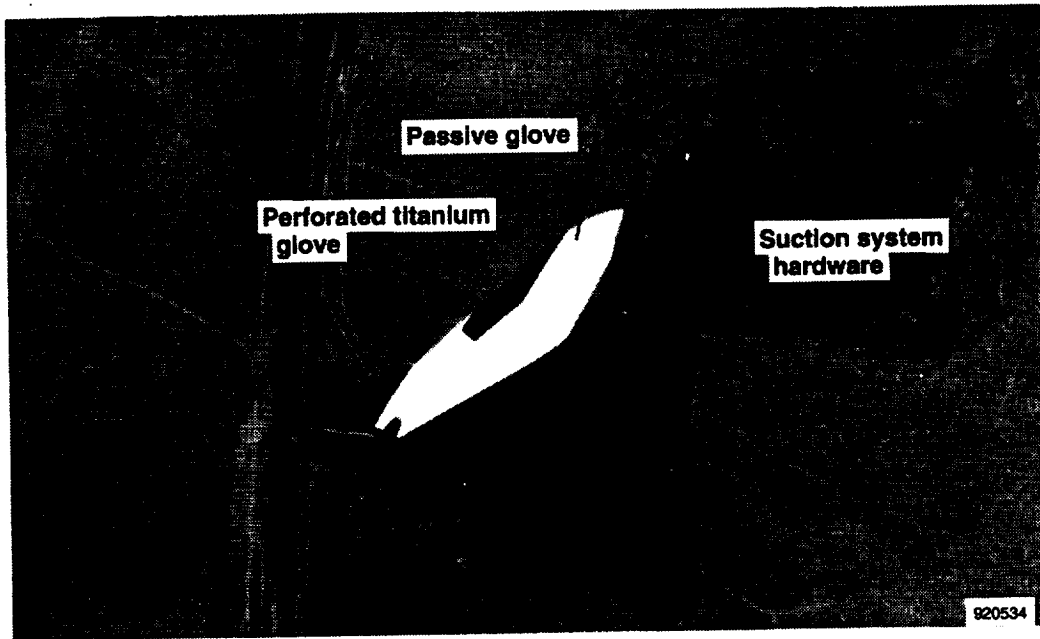


Fig. 17 Laminar flow control experiment installed on F-16XL.

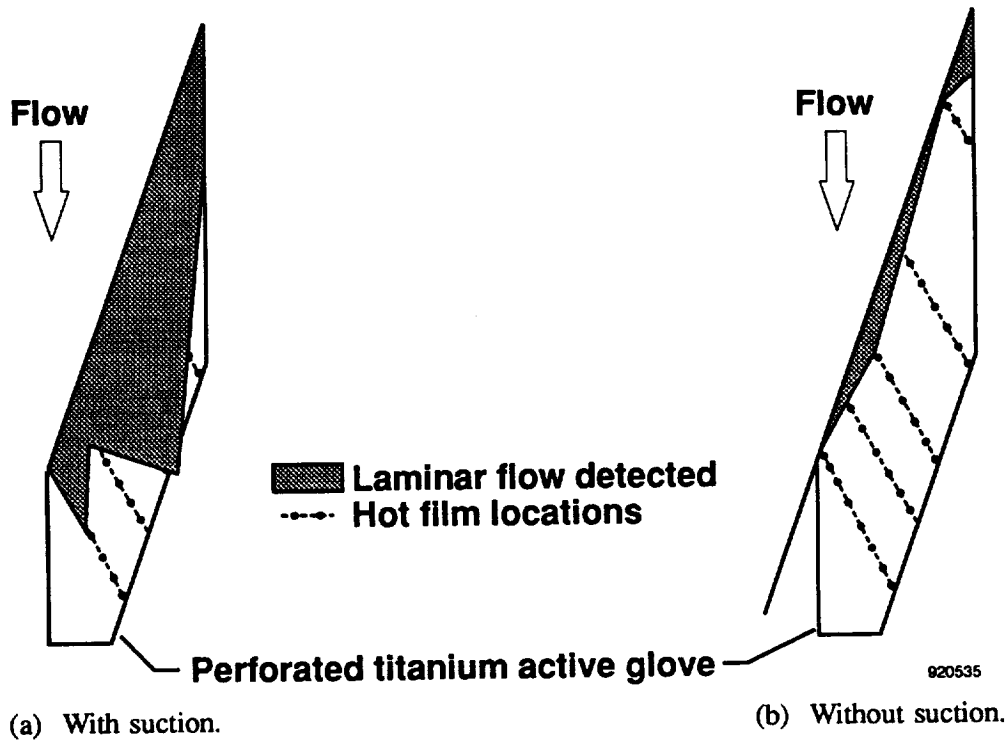


Fig. 18 Laminar flow control experiment results from the F-16XL, $M > 1$ and $\Lambda = 70^\circ$.

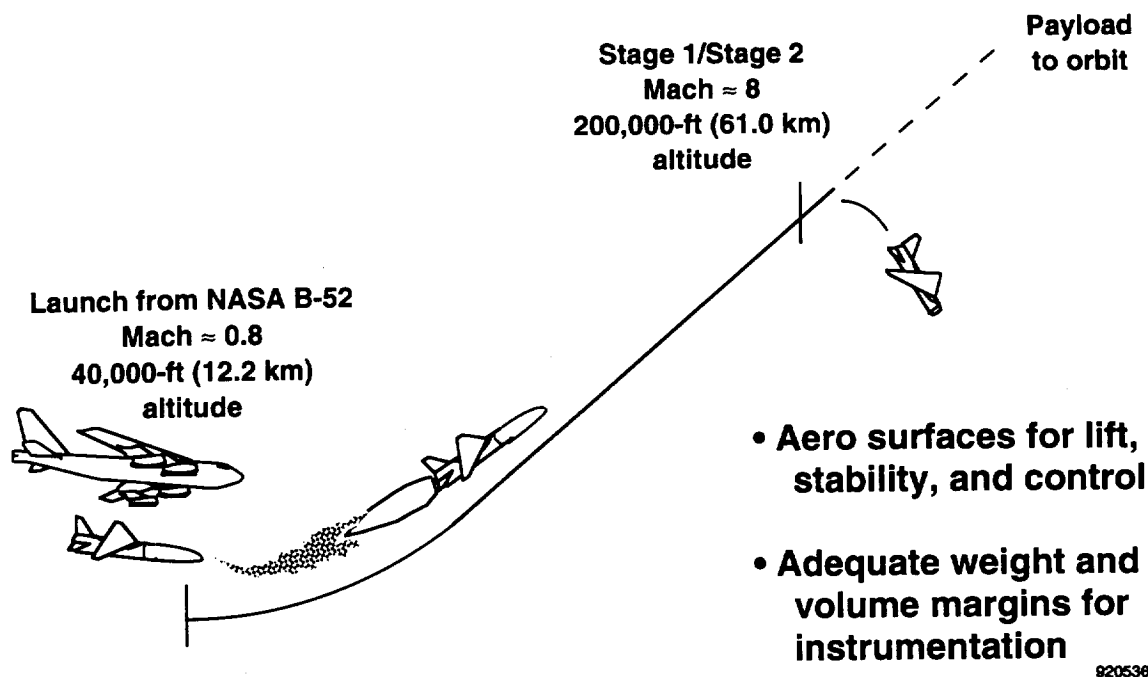


Fig. 19 Pegasus first stage add-on hypersonic research experiment description.

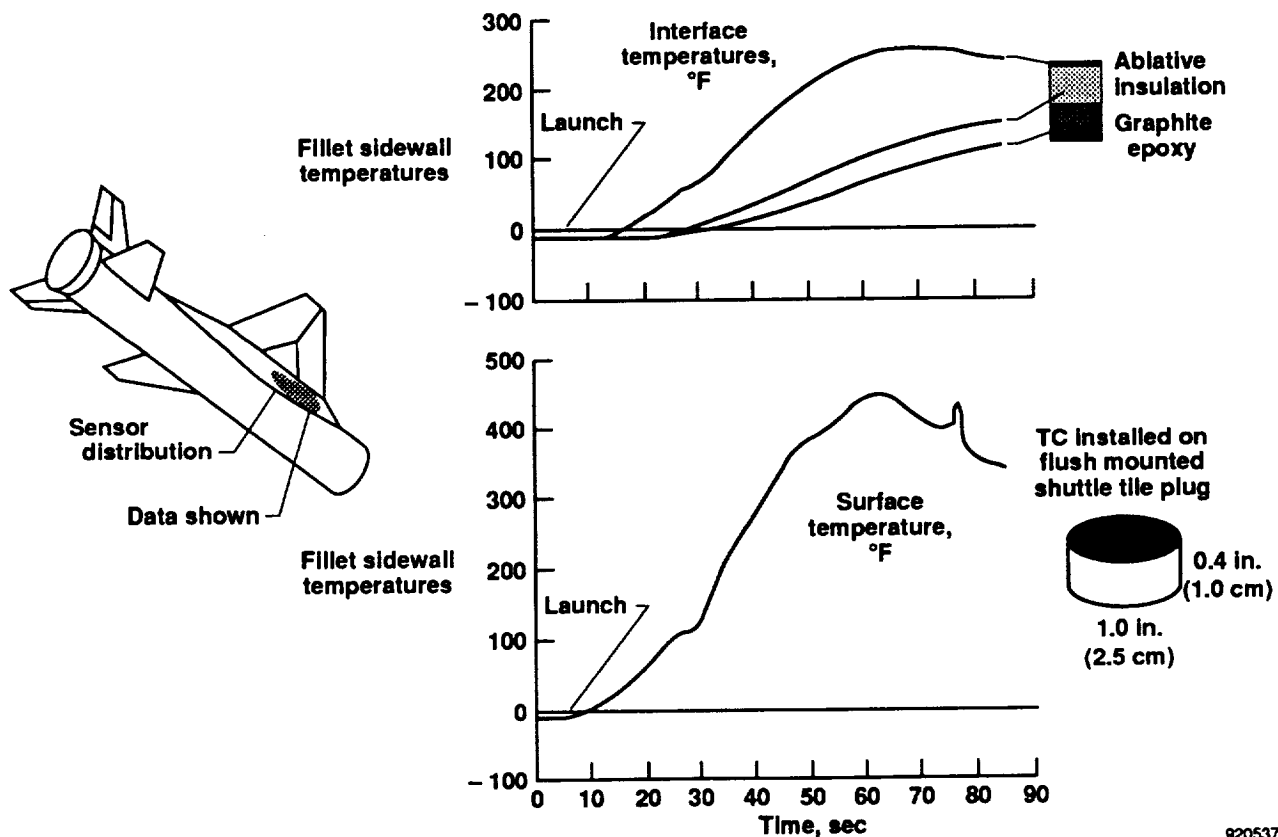


Fig. 20 Typical hypersonic research results obtained from Pegasus first stage temperature measurements.

REPORT DOCUMENTATION PAGEForm Approved
OMB No. 0704-0188

Public reporting burden for this collection of information is estimated to average 1 hour per response, including the time for reviewing instructions, searching existing data sources, gathering and maintaining the data needed, and completing and reviewing the collection of information. Send comments regarding this burden estimate or any other aspect of this collection of information, including suggestions for reducing this burden, to Washington Headquarters Services, Directorate for Information Operations and Reports, 1215 Jefferson Davis Highway, Suite 1204, Arlington, VA 22202-4302, and to the Office of Management and Budget, Paperwork Reduction Project (0704-0188), Washington, DC 20503.

1. AGENCY USE ONLY (Leave blank)		2. REPORT DATE August 1992	3. REPORT TYPE AND DATES COVERED NASA Technical Memorandum	
4. TITLE AND SUBTITLE Overview of the NASA Dryden Flight Research Facility Aeronautical Flight Projects			5. FUNDING NUMBERS WU 505-68-50	
6. AUTHOR(S) Robert R. Meyer				
7. PERFORMING ORGANIZATION NAME(S) AND ADDRESS(ES) NASA Dryden Flight Research Facility P.O. Box 273 Edwards, California 93523-0273			8. PERFORMING ORGANIZATION REPORT NUMBER H-1847	
9. SPONSORING/MONITORING AGENCY NAME(S) AND ADDRESS(ES) National Aeronautics and Space Administration Washington, DC 20546-0001			10. SPONSORING/MONITORING AGENCY REPORT NUMBER NASA TM-104254	
11. SUPPLEMENTARY NOTES Presented as AGARD paper 16 at the AGARD Flight Mechanics Panel, Chania, Crete, Greece, May 11, 1992.				
12a. DISTRIBUTION/AVAILABILITY STATEMENT Unclassified — Unlimited Subject Category 05			12b. DISTRIBUTION CODE	
13. ABSTRACT (Maximum 200 words) Several principal aeronautics flight projects of the NASA Dryden Flight Research Facility are discussed. Key vehicle technology areas from a wide range of flight vehicles are highlighted. These areas include flight research data obtained for ground facility and computation correlation, applied research in areas not well suited to ground facilities (wind tunnels), and concept demonstration.				
14. SUBJECT TERMS Flight test, Flow visualization, High angle of attack, Propulsion optimization flight-test techniques, Supersonic laminar flow			15. NUMBER OF PAGES 20	
			16. PRICE CODE A02	
17. SECURITY CLASSIFICATION OF REPORT Unclassified	18. SECURITY CLASSIFICATION OF THIS PAGE Unclassified	19. SECURITY CLASSIFICATION OF ABSTRACT Unclassified	20. LIMITATION OF ABSTRACT Unlimited	